RESEARCH ARTICLE | AUGUST 22 2025

Scaling laws for electroosmotic flow of power-law fluids in fractal branching networks

Ashish Garg

Physics of Fluids 37, 082137 (2025)
https://doi.org/10.1063/5.0282910

Physics of Fluids ARTICLE pubs.aip.org/aip/pof

Scaling laws for electroosmotic flow of power-law fluids in fractal branching networks

Cite as: Phys. Fluids **37**, 082137 (2025); doi: 10.1063/5.0282910
Submitted: 28 May 2025 · Accepted: 30 July 2025 ·
Published Online: 22 August 2025

Ashish Garg[1,2,a)]

AFFILIATIONS

[1]Department of Chemical Engineering, Indian Institute of Technology Delhi, Delhi 110016, India
[2]Soft Condensed Matter Group, Raman Research Institute, Bengaluru 560080, Karnataka, India

[a)]**Author to whom correspondence should be addressed:** ashish.garg.iisc@gmail.com and ashish@seminare.in

ABSTRACT

Electroosmotic flow (EOF) plays a vital role in fluid transport within micro- and nano-scale systems handling ionic fluids. Driven by electric fields and resisted by viscous forces, EOF is especially relevant for microfluidic applications. This study presents the theoretical framework for EOF of power-law fluids in fractal-like branching networks, addressing both volume and surface-area constraints, a domain unexplored in existing literature on flow optimization. Prior EOF analyses have focused on Newtonian fluids in fractal networks or numerical analysis of power-law fluid flows in complex geometries; here, we extend the scope to non-Newtonian fluids and complex hierarchies using theory and derived scaling laws. Assuming fully developed, steady, axisymmetric, and incompressible EOF in cylindrical microchannels, the model incorporates the Debye–Hückel approximation to linearize electrokinetic behavior and neglects pressure-driven components. The resulting electroosmotic flow rates Q for power-law fluid enhance for shear-thinning fluids (lower n) compared to Newtonian or shear-thickening fluids. Under volume constraints, we show that the optimal branching radius ratio β^* scales as $N^{-1/2}$, yielding uniform mean velocity across all generations. This configuration yields a maximum normalized conductance $E_{\text{vol}} = 1$, independent of the number of bifurcations N, length ratio γ, or generation count m. Under surface-area constraints, β^* scales as $N^{-(n+1)/(2n+1)}$, where n is the power-law index. Here, optimal transport depends on n and N, with conductance E_{surf} decreasing as γ, n, m, or N increases. These novel scaling laws, reported for the first time for electroosmotic flow of power-law fluids in branching networks, underscore the fundamental differences between electroosmotic and pressure-driven flows. The results offer novel, valuable insights for designing bioinspired microfluidic designs, electrokinetic pumps, and lab-on-a-chip devices. This work bridges fluid rheology with network geometry, offering a rigorous theoretical foundation for efficient EOF transport.

NOMENCLATURE

Symbol

ΔV	Applied electric potential difference (V)
ϵ_0	Vacuum permittivity (F/m)
ϵ_r	Relative permittivity
ζ	Zeta potential (V)
η_0	Consistency factor of the viscosity (Pa·s^n)
λ_D	Debye length (m)
A_k	Cross-sectional area of generation k (m^2)
k	Branching generation index
L	Channel length (m)
L_k	Length of channels in generation k (m)
n	Power-law index (rheology parameter)
Q	Electroosmotic volumetric flow rate (m^3/s)
Q_k	Flow rate in generation k (m^3/s)
R	Channel radius (m)
R_k	Radius in generation k (m)
u_z	Axial velocity (m/s)

I. INTRODUCTION

The widespread adoption of microfluidic devices across diverse scientific domains stems from their advantageous features, such as high surface-to-volume ratios and enhanced rates of heat and mass transfer. These characteristics facilitate efficient chemical separations, rapid reactions, sensitive detections, and improved operational safety.[1,2] Microfluidic systems find critical applications in micro-total analysis systems for DNA sequencing, biosensing, targeted drug delivery,[3,4] and thermal management of compact electronic circuits.[5]

Among the various transport mechanisms in microfluidics, electroosmotic flow (EOF) is a fundamental electrokinetic phenomenon

widely employed in microfluidic and nanofluidic systems, particularly for manipulating ionic solutions in confined geometries. Unlike pressure-driven flows that rely on mechanical pumps, EOF is induced by the interaction between an applied electric field and the electrical double layer (EDL) formed at the solid–liquid interface. This mechanism enables precise, silent, and valve-less control of fluid motion, making it especially attractive for lab-on-a-chip technologies, biomedical diagnostics, and chemical separation processes.[6–10]

Recent studies have extended the utility of electroosmotic phenomena to a wide range of advanced applications. These include nanoparticle-laden flows in biomedical microchips,[6,11] electrokinetically-driven nanofluid-based cooling systems,[6,12] and ionic microreactors where nanoparticle suspensions exhibit non-Newtonian electrolyte behavior.[6,13] The ability to predict optimal electroosmotic performance in such systems is essential for enhancing energy conversion, diagnostics, and targeted drug delivery at the microscale.[6,11]

However, most EOF-based scaling laws and flow analyses have traditionally assumed Newtonian fluid behavior, which does not reflect the rheological complexity of many real-world fluids, such as polymer solutions, biological specimens, and colloidal dispersions that exhibit non-Newtonian characteristics. Among various rheological models, power-law fluids offer a simple yet effective means of modeling shear-dependent viscosity, described by the relation $\boldsymbol{\tau} = \eta_0 |\dot{\gamma}|^{n-1}\dot{\gamma}$, where n is the flow behavior index.[14] These fluids demonstrate distinct electroosmotic behavior, including shear-thinning for $n < 1$, Newtonian for $n = 1$, and shear-thickening for $n > 1$.

Several researchers have explored the implications of such non-Newtonian effects in microfluidic electrokinetics. Zhao and Yang[15] analyzed power-law fluid flow in single microchannel with electrokinetic effects and derived analytical solutions for specific cases with $n = 1$, $1/2$, and $1/3$. Bharti *et al.*[16] numerically examined electroviscous influences in fully developed, pressure-driven flows of power-law fluids in single circular microchannel. Vasu and De[17] extended the analysis to EOF of power-law fluids in slit microchannels, especially under high zeta potentials, and also studied pressure-driven flows using the Debye–Hückel approximation,[18] focuses on the formation and characteristics of stationary planes during EOF. Additionally, Srinivas[19] performed numerical simulations of EOF in elliptical geometries to highlight shape-induced effects.

Further studies found that the rheology changes the dynamics of EOF. For instance, under alternating current (AC) fields, shear-thinning fluids demonstrate accelerated transient responses and larger velocity amplitudes due to reduced viscous resistance.[20] In another investigation of electroosmotic flow of an Oldroyd-B fluid over asymmetrically charged surfaces in microchannels. The study reveals how surface charge modulation and viscoelasticity significantly alter slip velocity, flow symmetry, and net throughput.[21] Further, Jing and Qi[22] numerically found that the electroosmotic flow (EOF) in fractal tree-like convergent microchannel networks. They analyzed how geometric parameters such as branch convergence, branching number, and channel height, affect flow rate and resistance. The paper identifies optimal fractal tree-like convergent microchannel network structures for maximizing EOF transport efficiency, aiding in microfluidic design. Furthermore, Jing and Zhan[23] found that for Newtonian fluids, the dependence of EOF fluidic resistance in a symmetric fractal rectangular microchannel network is governed primarily by the channel width as $\kappa = N^{-1}$ when the total channel volume is conserved, where N is the branching number. In contrast, under surface area constraint, the optimal cross-sectional dimensions must satisfy both width $\kappa = N^{-1}$ and height $H = \frac{S}{4l_0} \cdot \frac{1-\gamma^N}{(1-\gamma)(N\kappa)^m}$, where γ is the length ratio and m is the total branching levels. Similarly, in another study by Jing and Yi[24] found the optimal radius ratio for EOF of Newtonian fluid under volume constraint to be equal to $N^{-1/2}$. In addition, Jing *et al.*[25] revised Murray's law[26] by incorporating surface charge-induced electroviscous effects in fractal tree-like microchannel networks. It showed that both zeta potential and microchannel radius caused non-monotonic variations in the optimal branching radius ratio. The optimal design for minimizing hydraulic resistance depended on the apparent electroviscosity and channel length ratio across successive branching levels. Moreover, in another numerical study by Choi *et al.*[27] found EOF of non-Newtonian power-law fluids in rectangular microchannels that the shear-thinning fluids (lower behavior index) enhance flow. Higher flow is observed when the bottom surface has a strong zeta potential and side walls are present. Further, Choi *et al.*[28] found an approximate solution for the EOF of power-law fluids in a planar single microchannel, with thinning enhances the flow. We clearly can guess that these rheological effects could further complicate in fractal branching networks, ubiquitous in biological systems (e.g., vascular networks) and engineered devices, where self-similar bifurcations optimize transport efficiency under physical constraints. From the literature, it has been found that prior EOF analyses have focused on Newtonian fluids in fractal networks or numerical analysis of power-law fluid flows in complex geometries.

This study explores the EOF of power-law fluids in fractal-like branching networks. These networks exhibit a hierarchical, fractal, self-similar branching network composed of axisymmetric cylindrical microchannels, mimics natural and engineered transport systems frequently encountered in biomedical and microscale engineering applications. The underlying structure is designed to emulate multi-generational bifurcating microchannel arrays, similar to those found in biological vasculature (e.g., bronchial trees, arterial networks) or artificial microfluidic devices for lab-on-a-chip technologies.

In the context of an engineering process, Fig. 1 illustrates an ink-jet printing system that utilizes electroosmotic flow (EOF) for precise ink ejection. At the top, an ink reservoir supplies the ink to a printhead assembly. Within the printhead, there are multiple individual channels, each acting as a nozzle. At the top of each channel, electrodes are positioned, connected to a power source. These electrodes apply an electric field across the ink within the nozzle channels. This electric field interacts with charges on the channel walls and within the ink, generating electroosmotic flow, which precisely propels the ink downward. By controlling the electric field at each nozzle, the system can selectively eject individual ink droplets onto a selective nozzle on the substrate below, forming desired patterns or images through the controlled deposition of different colored inks, as shown.

The fractal domain geometry, represented schematically in Fig. 2, allows uniform distribution of flow or electric field intensity when optimized properly. The analytical model captures how the radius R_k, length L_k, and zeta potential ζ vary spatially under volume or surface constraints. This is crucial for devices such as electrokinetic micropumps, electroosmotic mixers, or heat exchangers using nanofluids, where flow uniformity and energy efficiency depend on precise geometry–flow coupling.

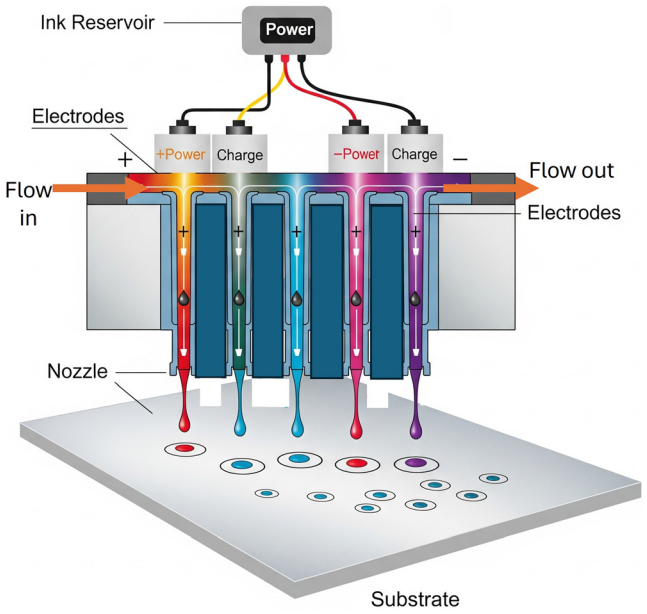

FIG. 1. This figure illustrates an inkjet printing system that leverages electroosmotic flow (EOF) for precise ink ejection. An ink reservoir feeds into a printhead with multiple nozzles. Electrodes at each nozzle generate an electric field, which interacts with charged ink molecules and channel walls to create EOF, propelling ink droplets downward. Depending on the electric field at each nozzle, this controlled EOF allows for selective and precise deposition of different colored ink droplets onto a substrate.

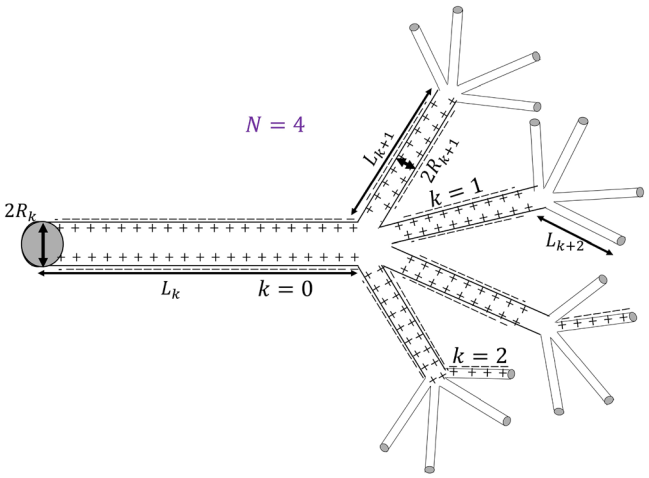

FIG. 2. Schematic of electroosmotic flow of power-law fluids in a fractal self-similar network of circular cross section. Here, N is the splitting at the junction and k is generations. R_k is the radius at k_{th} generation.

However, to date, there has been no comprehensive analytical framework that integrates electroosmotic transport, power-law rheology, and fractal geometry under design constraints such as fixed volume or surface area. Here, in this paper, we extend the scope to non-Newtonian fluids and complex hierarchies using theory and derived scaling laws under both the volume and the surface-area constraint. These scaling principles extend Murray's law (originally for blood vessels)[29] to electrokinetic systems, minimizing flow resistance while maximizing conductance. By mathematically modeling the domain under steady, fully developed EOF and accounting for power-law fluid behavior, this study provides an engineering framework to directly guide the fabrication of fractal microchannel systems with optimized performance metrics such as conductance, velocity uniformity, and energy efficiency.

The model presented in this study offers the theoretical framework that couples electroosmotic transport with power-law fluid rheology in hierarchically branching networks under specific physical constraints (volume or surface area). Unlike earlier studies confined to Newtonian fluids or numerically-intensive simulations, our analytical treatment yields closed-form scaling laws applicable to a wide range of fluid index n for bioinspired and engineered microfluidic designs.

Our work derives novel scaling laws for optimized EOF transport, demonstrating that the optimal branching radius ratio is uniquely influenced by the number of bifurcations and fluid rheology. We analytically show that under a volume constraint, an optimal radius ratio of $\beta^* = N^{-1/2}$ results in a universal geometrical design, ensuring uniform mean velocity and maximal normalized conductance irrespective of network specifics or fluid power-law index. Conversely, under a surface-area constraint, we discover that the optimal branching ratio follows $\beta^* = N^{-(n+1)/(2n+1)}$, highlighting a strong dependence of conductance on both the power-law index n and network complexity. Ultimately, this research establishes critical relationships between network geometry, fluid rheology, and EOF transport efficiency. By generalizing electroosmotic transport through self-similar networks, the model not only advances fundamental understanding but also provides optimization guidelines critical for device-level implementations such as electrokinetic drug delivery, lab-on-a-chip flows, and nanofluidic heat exchangers.

The governing equations are derived from the Poisson–Boltzmann and Navier–Stokes formulations, simplified under the Debye–Hückel approximation, which assumes a low surface potential and thin EDL. Flow within the EDL is considered negligible, and the system is driven purely by the electric field, with no applied pressure gradient. A schematic is shown in Fig. 2.

II. THEORETICAL MODEL FOR ELECTROOSMOTIC POWER-LAW FLUID FLOW IN THE FRACTAL NETWORK

A. Governing equations

Electroosmotic flow (EOF) occurs when an external electric field drives a fluid containing positive and negative ions along a charged cylindrical surface. In this study, we consider EOF inside a cylindrical microchannel of radius R and length L filled with an electrolyte solution. The outer/inner surface of the cylinder carries a uniform negative/positive charge, leading to the formation of a zeta potential, denoted as ζ, which is assumed to be uniform along the axial (z) direction as shown in Fig. 3 for a single tube. The electrostatic interactions between the charged surface and the ions in the electrolyte result in the formation of an electrical double layer (EDL) near the charged cylindrical surface.

We assume that the flow is fully developed, steady, and governed by the Stokes equation since the Reynolds number is significantly less

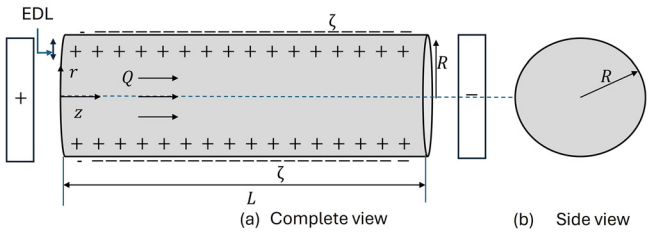

FIG. 3. Schematic diagram of the electroosmotic flow in a single tube of radius R and length L. ζ is the potential applied at the surface. EDL is the electrical double layer (EDL) length within which the electrical potential varies.

than one, i.e., $Re \ll 1$. Therefore, the inertial forces are negligible compared to viscous forces. This assumption holds for electroosmotic flows in cylindrical microchannels due to typically low fluid velocities. The momentum and continuity equation under Stokes flow in cylindrical coordinates is given by

$$0 = -\nabla p + \nabla \cdot \boldsymbol{\tau} + \rho_f \boldsymbol{E}, \tag{1a}$$

$$\nabla \cdot \boldsymbol{u} = 0, \tag{1b}$$

where $\boldsymbol{u}$ and $\boldsymbol{\tau}$ are the velocity vector and stress tensor, respectively. p and ρ_f are the pressure and net charge density, respectively. The electric field is related to the potential ϕ as

$$\boldsymbol{E} = -\nabla \phi. \tag{2}$$

B. Boundary conditions

The impermeable and no-slip condition at the wall ensures

$$\boldsymbol{u} \cdot \mathbf{n}_{\text{wall}} = 0, \quad \boldsymbol{u} \cdot \mathbf{t}_{\text{wall}} = 0, \tag{3}$$

where $\mathbf{n}_{\text{wall}}$ and $\boldsymbol{t}_{\text{wall}}$ are the unit normal and tangential vectors at the boundary. At the centerline, symmetry dictates

$$\boldsymbol{u} \cdot \mathbf{n}_{\text{centerline}} = 0, \quad \boldsymbol{t} \cdot \mathbf{m}_{\text{centerline}} = 0, \tag{4}$$

where $\mathbf{t}$ is the traction on the wall. The velocity gradients vanish at the centerline ($r = 0$) due to symmetry. Further, far from the charged wall outside EDL, which is of order of a few nanometers $O(10\,\text{nm})$ (i.e., toward the center of the channel for large r), the equilibrium potential due to the EDL formation tends to zero.

C. Power-law fluids

We model the power-law fluid as[30]

$$\boldsymbol{\tau} = \eta_o |\dot{\boldsymbol{\gamma}}|^{n-1} \dot{\boldsymbol{\gamma}} \quad \text{where} \quad \eta(\eta_o, n, |\dot{\boldsymbol{\gamma}}|) = \eta_o |\dot{\boldsymbol{\gamma}}|^{n-1}, \tag{5}$$

where $\eta(\eta_o, n, |\dot{\boldsymbol{\gamma}}|)$, $\boldsymbol{\tau}$, and $\dot{\boldsymbol{\gamma}}$ are the viscosity, the stress tensor (or τ in 1D), and the strain-rate tensor (or $\dot{\gamma}$ in 1D), respectively. Further, η_o and n are the consistency factor and power-law index, respectively. Furthermore, $|\dot{\boldsymbol{\gamma}}|$ is the strain rate invariant (or $|\dot{\gamma}|$ in 1D). In the stress strain-rate relation $\boldsymbol{\tau} = \eta(\eta_o, n, |\dot{\boldsymbol{\gamma}}|)\dot{\boldsymbol{\gamma}}$, the strain-rate tensor is

$$\dot{\boldsymbol{\gamma}} = ((\nabla \boldsymbol{v}) + (\nabla \boldsymbol{v})^T)$$

$$= \begin{bmatrix} 2\dfrac{\partial u_r}{\partial r} & \dfrac{\partial u_\theta}{\partial r} + \left(\dfrac{1}{r}\dfrac{\partial u_r}{\partial \theta} - \dfrac{u_\theta}{r}\right) & \dfrac{\partial u_r}{\partial z} + \dfrac{\partial u_z}{\partial r} \\ \dfrac{\partial u_\theta}{\partial r} + \left(\dfrac{1}{r}\dfrac{\partial u_r}{\partial \theta} - \dfrac{u_\theta}{r}\right) & 2\left(\dfrac{1}{r}\dfrac{\partial u_\theta}{\partial \theta} + \dfrac{u_r}{r}\right) & \dfrac{\partial u_\theta}{\partial z} + \dfrac{1}{r}\dfrac{\partial u_z}{\partial \theta} \\ \dfrac{\partial u_r}{\partial z} + \dfrac{\partial u_z}{\partial r} & \dfrac{\partial u_\theta}{\partial z} + \dfrac{1}{r}\dfrac{\partial u_z}{\partial \theta} & 2\dfrac{\partial u_z}{\partial z} \end{bmatrix}. \tag{6}$$

Despite its broad relevance, the power-law model, employed in this study to represent non-Newtonian fluid behavior, does come with certain well-recognized limitations. It does not capture yield stress effects present in Herschel–Bulkley fluids, nor does it reflect viscosity plateaus at very low or high shear rates. For shear-thinning fluids ($n < 1$), it predicts unphysically infinite viscosity as shear rate approaches zero, making it unsuitable for low-shear regimes. More comprehensive models, such as the Carreau–Yasuda, Cross, Bingham, or viscoplastic and thixotropic formulations, may better represent the full rheological complexity, particularly for time-dependent or elastic effects.

Despite its limitations, the power-law model continues to serve as an analytically convenient and widely utilized framework for capturing non-Newtonian behavior in many applications. It captures key shear-dependent features of numerous real fluids, such as blood, polymer solutions, and suspensions like ketchup or paint, within moderate shear-rate ranges. In our work, the power-law model is not intended as a precise fit to a particular material, but rather as a simplified yet insightful tool to explore the influence of nonlinearity in viscosity under electrokinetic effects, particularly in complex geometries such as branching networks. Its simplicity enables the derivation of analytical solutions and scaling laws, offering a tractable route to understand fundamental flow behavior that can later be refined using more sophisticated rheological models.

Moreover, even in more advanced models such as the Herschel–Bulkley or viscoelastic frameworks, the power-law formulation is often embedded as a constitutive backbone, especially in the regime above the yield stress or at low Deborah numbers. In shear-thickening fluids ($n > 1$), while real behaviors are more intricate, the power-law approximation is frequently employed piecewise to represent distinct thinning and thickening regions.

D. Axisymmetric model

The analytical approach employed in this study is based on classical electrokinetic theory, integrating the linearized Poisson–Boltzmann equation with the Stokes equations to model low Reynolds number flow of power-law fluids. The development of an axisymmetric model is motivated by the need for closed-form scaling laws that remain valid across multiple branching generations and a broad range of fluid rheologies. Unlike previous studies that often derive analytical solutions only for specific values of the flow behavior index n, the present formulation retains generality for any n, thereby offering greater flexibility and applicability for non-Newtonian systems.

Unlike numerical techniques such as finite element or finite volume methods, which are computationally intensive and often case-specific, the analytical framework enables the derivation of explicit

expressions for flow velocity, conductance, and optimal geometry. These results provide direct physical insight and design relevance, particularly under practical constraints such as fixed network volume or surface area.

Although more comprehensive models, such as those incorporating the full Poisson–Nernst–Planck system or nonlinear electric double layer (EDL) effects exist, they are often less suited for extracting universal design principles with closed-form solutions and are unable to retain generality. Therefore, the present methodology offers a balanced solution: mathematically tractable, physically representative, and broadly applicable to microfluidic systems involving non-Newtonian fluids.

To derive the axisymmetric model from the Stokes equations (1), the following assumptions are considered as

- $\frac{\partial}{\partial\theta}() = 0$ for assuming axisymmetry.
- No variation in pressure/stress along the azimuthal direction, which gives $u_\theta = 0$.
- We assume steady flow, which means $\frac{\partial}{\partial t}() = 0$.
- We assume a fully developed velocity profile along the axial direction, which means, $\frac{\partial}{\partial z}(\boldsymbol{u}) = 0$.
- Incompressible, EOF with no gravitational forces, and no losses near the branch splitting or any secondary flows.
- No pressure gradient in any direction.

The laminar electroosmotic flow in a circular tube with radius R is shown in Fig. 3. We assume the velocity u_z and u_r, along the axial (z) and radial directions (r), respectively, with the r measured from the center of the tube. Using the assumptions with an impermeable wall, we get, $u_r(r = R) = 0$, from the continuity equation, and also we get the radial velocity vanishes everywhere,[31] i.e.,

$$u_r(r, t) = 0. \tag{7}$$

Further assuming lubrication approximations and using the boundary condition, the axial direction equation for an axisymmetric system becomes

$$0 = -\frac{\partial p}{\partial z} + \frac{1}{r}\frac{d}{dr}(r\tau_{rz}) + \rho_f E_z, \tag{8}$$

where $\frac{\partial p}{\partial z} = 0$ as no pressure gradient is applied. The electric field is related to the electrostatic potential ϕ as

$$E_z = -\frac{\partial \phi}{\partial z}. \tag{9}$$

The electrostatic potential ϕ consists of two components as

$$\phi = -E_0 z + \phi_{eq}(r), \tag{10}$$

where E_0 is the externally applied uniform electric field along the z-direction, and $\phi_{eq}(r)$ is the equilibrium potential due to the EDL. The charge density ρ_f is determined from Poisson's equation as[32]

$$\rho_f = -\epsilon\nabla^2\phi, \tag{11}$$

where ϵ is the permittivity of the fluid, further Eq. (11) becomes in cylindrical coordinates as

$$-\epsilon\left(\frac{1}{r}\frac{d}{dr}\left(r\frac{d\phi_{eq}}{dr}\right)\right) = \rho_f. \tag{12}$$

For a power-law fluid, the constitutive equation relating the shear stress τ_{rz} and the velocity gradient is given by

$$\tau_{rz} = \eta_o\left|\frac{du_z}{dr}\right|^{n-1}\frac{du_z}{dr}, \tag{13}$$

where $n < 1$ for shear-thinning fluids, $n = 1$ for Newtonian fluids, and $n > 1$ for shear-thickening (dilatant) fluids. Thus, the governing equation for electroosmotic flow simplifies to

$$\frac{1}{r}\frac{d}{dr}\left(r\eta_o\left|\frac{du_z}{dr}\right|^{n-1}\frac{du_z}{dr}\right) = \epsilon E_0\frac{1}{r}\frac{d}{dr}\left(r\frac{d\phi_{eq}}{dr}\right). \tag{14}$$

The boundary conditions for the velocity profile and for the electrostatic potential are

$$u_z(r = R) = 0 \quad (\text{No} - \text{slip condition}), \quad \phi_{eq}(r = R) = \zeta, \tag{15}$$

$$\frac{du_z}{dr} = 0, \quad \phi_{eq}(r = 0) = 0 \quad \text{at} \quad r = 0. \tag{16}$$

Integrating once, we get

$$\eta_o r\left(-\frac{du_z}{dr}\right)^{n-1}\frac{du_z}{dr} = \epsilon E_0 r\frac{d\phi_{eq}}{dr} + C_1. \tag{17}$$

Applying the boundary condition at $r \to 0$, we get $C_1 = 0$. Further, $\dot{\gamma} = \frac{\partial u_z}{\partial r}$. Additionally, as radius r increases, the velocity decreases; therefore, a negative sign is introduced in the bracket in order to remove the modulus. After rearranging, we get

$$-\left(-\frac{du_z}{dr}\right)^n = \frac{\epsilon E_0}{\eta_o}\frac{d\phi_{eq}}{dr}. \tag{18}$$

Taking the nth root on both sides gives

$$-\frac{du_z}{dr} = \left(\frac{-\epsilon E_0}{\eta_o}\frac{d\phi_{eq}}{dr}\right)^{\frac{1}{n}}. \tag{19}$$

Integrating both sides gives

$$-\int du_z = \int\left(\frac{-\epsilon E_0}{\eta_o}\frac{d\phi_{eq}}{dr}\right)^{\frac{1}{n}}dr. \tag{20}$$

As we know, in a circular pipe of radius R, the equilibrium electrostatic potential $\phi_{eq}(r)$ in the presence of an electrical double layer (EDL) is governed by the Poisson–Boltzmann equation. For small zeta potential ($\zeta e/kT \ll 1$, Debye–Hückel approximation[32]) the linearized form of the Poisson–Boltzmann equation in cylindrical coordinates (r-direction) can be written as

$$\frac{1}{r}\frac{d}{dr}\left(r\frac{d\phi_{eq}}{dr}\right) = \frac{\phi_{eq}}{\lambda_D^2}, \tag{21}$$

which has a general solution to this differential equation as

$$\phi_{eq}(r) = AI_0(r/\lambda_D) + BK_0(r/\lambda_D), \tag{22}$$

where I_0 and K_0 are the zeroth-order modified Bessel functions of the first and second kind, respectively. λ_D is the Debye length, which characterizes the thickness of the EDL. At the wall ($r = R$): the potential is

set to the zeta potential $\phi_{eq}(R) = \zeta$. At the pipe center ($r = 0$), outside the EDL, the solution must decay to zero, meaning we discard $K_0(r/\lambda_D)$ because it diverges at $r = 0$. Thus, the solution simplifies to[33]

$$\phi_{eq}(r) = \zeta \frac{I_0(r/\lambda_D)}{I_0(R/\lambda_D)}. \tag{23}$$

While the Bessel function does not have a simple closed-form expression, however, for large arguments ($x \gg 1$), the modified Bessel function $I_0(x)$ can be approximated by

$$I_0(x) \approx \frac{e^x}{\sqrt{2\pi x}}.$$

Therefore,

$$I_0(r/\lambda_D) \approx \frac{e^{r/\lambda_D}}{\sqrt{2\pi(r/\lambda_D)}}, \quad I_0(R/\lambda_D) \approx \frac{e^{R/\lambda_D}}{\sqrt{2\pi(R/\lambda_D)}}.$$

Thus, the equilibrium potential can be rewritten as

$$\phi_{eq}(r) \approx \zeta \frac{e^{r/\lambda_D}/\sqrt{r/\lambda_D}}{e^{R/\lambda_D}/\sqrt{R/\lambda_D}}.$$

For large R/λ_D, near the pipe wall $r \to R$, we can simplify this to

$$\phi_{eq}(r) \approx \zeta e^{(r-R)/\lambda_D}.$$

The approximation is valid for large R/λ_D, and mimics the exponential decay seen in planar geometries, where the potential decays as e^{-z/λ_D} away from a charged surface. The EDL is of the order of $O(10nm)$ or smaller, therefore, for a microchannel $R/\lambda_D \gg 1$. Substituting this into the integral, we get

$$-u_z = \int \left(\frac{-\epsilon E_0}{\eta_o}\frac{\zeta}{\lambda_D} e^{(r-R)/\lambda_D}\right)^{\frac{1}{n}} dr, \tag{24}$$

and after integrating, obtain

$$\begin{aligned} -u_z &= \left(\frac{-\epsilon E_0}{\eta_o}\frac{\zeta}{\lambda_D}\right)^{\frac{1}{n}} n\lambda_D\, e^{(r-R)/n\lambda_D} + C_2 \\ &= \left(\frac{-\epsilon E_0}{\eta_o}\frac{\phi_{eq}(r)}{\lambda_D}\right)^{\frac{1}{n}} n\lambda_D + C_2. \end{aligned} \tag{25}$$

Applying the boundary condition at $r = R$, $\phi_{eq}(R) = \zeta$, and $u_z = 0$, we get

$$u_z = n\lambda_D \left(\frac{-\epsilon E_0}{\eta_o}\frac{1}{\lambda_D}\right)^{\frac{1}{n}} \left(\zeta^{1/n} - (\phi_{eq}(r))^{1/n}\right). \tag{26}$$

Further, the voltage drop $\delta V = V_{z=0} - V_{z=L}$ across the pipe length L leads to a uniform electric field. Therefore, we can write

$$E_0 = \frac{V_{z=L} - V_{z=0}}{L} = -\frac{\Delta V}{L}.$$

Moreover, the permittivity of the liquid ϵ, can be written in terms of the vacuum permittivity ϵ_o and relative permittivity ϵ_r of the liquid as $\epsilon = \epsilon_o\epsilon_r$. Therefore, Eq. (26) can be written as

$$u_z = n\lambda_D \left(\frac{\epsilon_o\epsilon_r \Delta V}{L\eta_o}\frac{1}{\lambda_D}\right)^{\frac{1}{n}} \zeta^{1/n}\left(1 - e^{(r-R)/n\lambda_D}\right). \tag{27}$$

The Eq. (27) for the axial velocity u_z of electroosmotic flow can be interpreted inside and outside the electric double layer (EDL).

1. Within the electric double layer (EDL)

Thin region near the pipe wall for $R - \lambda_D \lesssim r < R$, the charge density is significant and electrostatic forces are actively driving the flow. The velocity grows from zero at the wall toward its maximum bulk value. The exponential term $e^{\frac{r-R}{n\lambda_D}}$ varies rapidly from 0 to nearly 1. This means velocity increases sharply within the EDL thickness from 0 up to a value close to

$$u_z \approx u_z^{\text{bulk}} = n\lambda_D \left(\frac{\epsilon_o\epsilon_r \Delta V}{L\eta_o\lambda_D}\right)^{\frac{1}{n}} \zeta^{1/n}.$$

2. Outside the electric double layer (in the bulk)

For $r < R - \lambda_D$, in the bulk region, the exponential decays to zero $e^{\frac{r-R}{n\lambda_D}} \approx 0$.

So the velocity reaches a uniform plug-like profile given by

$$u_z = u_z^{\text{bulk}} = n\lambda_D \left(\frac{\epsilon_o\epsilon_r \Delta V}{L\eta_o\lambda_D}\right)^{\frac{1}{n}} \zeta^{1/n}.$$

This is a characteristic of electroosmotic flow for Newtonian fluids, especially in low Reynolds number and thin EDL regimes, where the flow is nearly uniform plug-like outside the EDL. The EDL is of the order of $O(10\,\text{nm})$ or smaller; therefore, $R/\lambda_D \gg 1$, which gives the approximate total flow rate, which is mainly flowing within the bulk of a microchannel, can be written as

$$Q \approx Q^{\text{bulk}} = \pi R^2 u_z^{\text{bulk}} = \pi R^2 n\lambda_D \left(\frac{\epsilon_o\epsilon_r \Delta V}{L\eta_o\lambda_D}\right)^{\frac{1}{n}} \zeta^{1/n}. \tag{28}$$

To investigate the influence of the power-law index n on electroosmotic flow rate Q, the parameters used in the Fig. 4 include a tube radius $R = 50\,\mu\text{m}$, Debye length $\lambda_D = 10\,\text{nm}$, vacuum permittivity $\epsilon_o = 8.854 \times 10^{-12}\,\text{F/m}$, relative permittivity for water $\epsilon_r = 80$, varying applied voltage $\Delta V = 0 - 100\,\text{V}$, channel length $L = 1\,\text{mm}$, dynamic viscosity $\eta_o = 1\,\text{mPa}\cdot\text{s}$, and zeta potential $\zeta = 50\,\text{mV}$. The power-law index n is varied from 0.4 to 10 to capture both shear-thinning and shear-thickening behaviors. The resulting flow rates Q from Eq. (28) were plotted against n, demonstrating that shear-thinning fluids (lower n) yield enhanced electroosmotic transport compared to Newtonian or shear-thickening fluids as shown in Fig. 4.

Previous studies have highlighted the strong influence of fluid rheology on electroosmotic flow (EOF) dynamics. Numerical investigations by Zhao *et al.*[20] and Choi *et al.*[27] demonstrated that shear-thinning fluids enhance EOF due to reduced viscous resistance. Our analytical findings are consistent with these results, confirming that power-law fluids exhibit distinct flow behaviors governed by the flow behavior index n. Shear-thinning fluids ($n < 1$) yield higher flow rates owing to lower effective viscosity and flatter, plug-like velocity profiles, whereas shear-thickening fluids ($n > 1$) exhibit reduced EOF due to

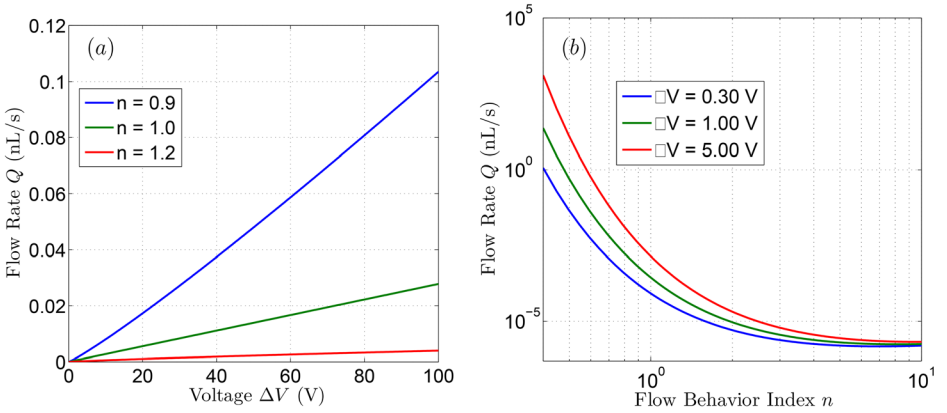

FIG. 4. Variation of electroosmotic volumetric flow rate Q with applied voltage ΔV and power-law index n is shown in panels (a) and (b), respectively. In (a), the flow rate increases with an increase in applied voltage ΔV for given n. Figure (b) demonstrating increased flow rates for shear-thinning fluids $n < 1$ and decreased flow for shear-thickening fluids $n > 1$, under identical electrokinetic and geometric conditions.

increased viscous resistance. The governing expression for the volumetric flow rate Q further highlights this trend, showing that Q increases as n decreases. These insights underscore the importance of accounting for fluid rheology when designing microfluidic systems, especially those involving complex fractal networks.

III. FLOW IN SELF-SIMILAR BRANCHING NETWORK

While electroosmotic flow (EOF) in straight or single channels is well understood for Newtonian fluids, the flow behavior in branched networks remains largely unexplored, specifically under generalized network conditions and different fluid rheology for shear-thinning and thickening fluids. We model and analyze how channel geometry, surface charge, and fluid rheology properties influence flow rate and distribution in hierarchically branching microchannels. The network considered consists of a series of bifurcating microchannels, where each branch divides into N daughter branches in successive generations, which varies from the initial $k = 0$ to the final generation level $k = m$. In this section, we calculate the total electroosmotic resistance and the corresponding normalized conductance in a tree-like circular tube network when subject to global volume and surface area constraints. These constraints are critical in both biological transport systems and miniaturized microfluidic devices, where material usage and device compactness must be optimized.

A. Flow resistance

The resistance $\mathcal{R}_k$ at the k_{th} generation level in the network is given by

$$\mathcal{R}_k = \frac{\Delta V_k}{Q_k^n} = \frac{L_k \eta_o \lambda_D}{\epsilon_o \epsilon_r (\pi R_k^2 n \lambda_D \zeta^{1/n})^n}, \tag{29}$$

where R_k and L_k are the radius and length of the pipe at the k_{th} generation level, respectively. At level k, the side and length scales as β and γ, respectively. Therefore,

$$R_k = R_0 \beta^k, \tag{30}$$

$$L_k = L_0 \gamma^k. \tag{31}$$

Here, R_0 and L_0 are the initial radius and length of the pipe at the starting 0_{th} generation level. Using these in Eq. (29) gives

$$\mathcal{R}_k = \frac{L_k \eta_o \lambda_D}{\epsilon_o \epsilon_r (\pi R_k^2 n \lambda_D \zeta^{1/n})^n} = \frac{L_0 \eta_o \lambda_D^{1-n}}{\zeta \epsilon_o \epsilon_r (\pi R_0^2 n)^n} \left(\frac{\gamma}{\beta^{2n}}\right)^k. \tag{32}$$

Thus, the total resistance $\mathcal{R}_t$ is

$$\mathcal{R}_t = \frac{1}{Q^n} \sum_{k=0}^{m} \Delta V_k. \tag{33}$$

Here, $k = 0$ and $k = m$ are the initial and final generation levels, respectively. A single branch splits into N new branches, creates N^k branches at k_{th} generation level. Thus, the total resistance is

$$\mathcal{R}_t = \frac{1}{Q^n} \sum_{k=0}^{m} \Delta V_k = \sum_{k=0}^{m} \frac{\mathcal{R}_k Q_k^n}{Q^n} = \frac{L_0 \eta_o \lambda_D^{1-n}}{\zeta \epsilon_o \epsilon_r (\pi R_0^2 n)^n} \sum_{k=0}^{m} \left(\frac{\gamma}{N^n \beta^{2n}}\right)^k$$

$$= \frac{L_0 \eta_o \lambda_D^{1-n}}{\zeta \epsilon_o \epsilon_r (\pi R_0^2 n)^n} \left(\frac{1 - \left(\frac{\gamma}{N^n \beta^{2n}}\right)^{m+1}}{1 - \frac{\gamma}{N^n \beta^{2n}}} \right), \tag{34}$$

where $Q = Q_k N^k$. Further, the total volume $\mathcal{V}$ and the total surface-area of the network is

$$\mathcal{V} = \sum_{k=0}^{m} N^k \pi (R_k)^2 L_k \quad \text{and} \quad \mathcal{S} = \sum_{k=0}^{m} 2 N^k \pi (R_k) L_k. \tag{35}$$

Utilizing the previously defined scaling and summing the series, we get

$$\mathcal{V} = \pi R_0^2 L_0 \frac{1 - (N\beta^2\gamma)^{m+1}}{1 - N\beta^2\gamma} \quad \text{and} \quad \mathcal{S} = 2\pi R_0 L_0 \frac{1 - (N\beta\gamma)^{m+1}}{1 - N\beta\gamma}. \tag{36}$$

B. Flow conductance *E* in fractal networks with volume and surface-area constraints

The equivalent single-tube length is

$$L_{\text{eq}} = \sum_{k=0}^{m} L_k = \sum_{k=0}^{m} L_0 \gamma^k = L_0 \frac{1 - \gamma^{m+1}}{1 - \gamma}. \tag{37}$$

Under the volume constraint, equating the total network volume $\mathcal{V}$ to that of an equivalent single tube, yields the radius of the equivalent single tube as

$$R_{\text{eq, vol}} = R_0 \left(\frac{1 - \gamma}{1 - \gamma^{m+1}} \frac{1 - (N\beta^2\gamma)^{m+1}}{1 - N\beta^2\gamma} \right)^{1/2}. \tag{38}$$

Equation (38) defines the radius of a hypothetical single conduit that maintains the same total volume and length as the entire fractal network. The corresponding flow resistance for this equivalent tube, preserving volume and length, is then given by

$$\mathcal{R}_{\text{eq, vol}} = \frac{\Delta V_k}{Q_k^n} = \frac{L_{\text{eq}}\eta_o\lambda_D^{1-n}}{\epsilon_o\epsilon_r\zeta(\pi R_{\text{eq, vol}}^2 n)^n} = \frac{L_0\eta_o\lambda_D^{1-n}}{\epsilon_o\epsilon_r\zeta(\pi R_0^2 n)^n}\left[\frac{1-\gamma^{m+1}}{1-\gamma}\right]^{(n+1)}\left[\frac{1-N\beta^2\gamma}{1-(N\beta^2\gamma)^{m+1}}\right]^n. \quad (39)$$

The dimensionless conductance under a fixed volume constraint, denoted as E_{vol}, is formulated as the ratio between the total conductance of the network, $E_t = 1/\mathcal{R}_t$, and the conductance of an equivalent single conduit, $E_{\text{eq}} = 1/\mathcal{R}_{\text{eq, vol}}$, expressed as

$$E_{\text{vol}} = \frac{1/\mathcal{R}_t}{1/\mathcal{R}_{\text{eq, vol}}} = \left[\frac{1-\gamma^{m+1}}{1-\gamma}\right]^{(n+1)}\left[\frac{1-N\beta^2\gamma}{1-(N\beta^2\gamma)^{m+1}}\right]^n\left[\frac{1-\gamma/N^n\beta^{2n}}{1-(\gamma/N^n\beta^{2n})^{m+1}}\right]. \quad (40)$$

Furthermore, the equivalent tube radius under surface-area constraint is expressed as

$$R_{\text{eq, surf}} = R_0\left(\frac{1-\gamma}{1-\gamma^{m+1}}\frac{1-(N\beta\gamma)^{m+1}}{1-N\beta\gamma}\right). \quad (41)$$

Accordingly, the non-dimensional flow conductance under a surface-area constraint, denoted as E_{surf}, can be expressed as

$$E_{\text{surf}} = \frac{1/\mathcal{R}_t}{1/\mathcal{R}_{\text{eq, surf}}} = \left[\frac{1-\gamma^{m+1}}{1-\gamma}\right]^{(2n+1)}\left[\frac{1-N\beta\gamma}{1-(N\beta\gamma)^{m+1}}\right]^{(2n)}\left[\frac{1-\gamma/N^n\beta^{2n}}{1-(\gamma/N^n\beta^{2n})^{m+1}}\right]. \quad (42)$$

IV. RESULTS AND DISCUSSION

In this section, we examine how the normalized conductance E varies with the branching radius ratio β across the network. The analysis explores the influence of key parameters such as the length ratio γ, the number of daughter branches N, and the total number of generations m. The constraints on total volume or surface area, as discussed in Secs. IV A and IV B for volume-limited and surface-limited networks, respectively, enable the identification of optimal conditions for electroosmotic flow. In addition, generalized scaling laws characterizing optimal transport in such constrained networks are established in Secs. IV A 2 and IV B 2 for the cases of volume and surface-area constraints, respectively.

A. Volume constrained networks

Electroosmotic flow conductance E_{vol} in a tree-like circular tube network for power-law fluid flow will be investigated under a total volume constraint, where the sum of the volumes of all branches across generations remains constant. Under limiting cases, the results are validated with previous numerical simulations and scaling laws on the Newtonian fluids with limited network topology. The results demonstrate how the flow behavior is influenced by various network and fluid rheology parameters. This condition is critical in biological systems and microfluidic device designs where spatial constraints are significant.

1. *Effect of* γ, m, *and* N

Figure 5 illustrates the variation of normalized electroosmotic conductance E_{vol} of the network with the dimensionless branching radius ratio β for various conditions of varying length ratio γ (a)–(c), the generations m (d)–(e), and the branches splitting N (g)–(i) for power-law fluids at $n = 0.6$ (a), (d), and (g) for shear-thinning, $n = 1$ (b), (e), and (h) for Newtonian, and $n = 1.5$ (c), (f), and (i) for shear-thickening fluids.

The flow through the network is primarily driven by the applied electric field, while it is resisted by the viscous resistance due to fluid motion through the branched microchannels. Hence, the balance between the electroosmotic driving force and the viscous resistance dictates the flow behavior across the network. The figure shows a non-monotonic relationship between E_{vol} and β, indicating the existence of an optimal branching condition that maximizes conductance. At low β, the viscous resistance dominates and restricts electroosmotic flow. As β increases, EOF becomes more efficient, which depends on network parameters.

For very small values of the radius ratio ($\beta \approx 0$), the normalized electroosmotic conductance E_{vol} approaches zero, regardless of the power-law index n, length ratio γ, branching level m, or bifurcation number N. This represents the minimum conductance. As the fluid becomes more shear-thickening (i.e., with increasing n), this low-conductance regime ($E_{\text{vol}} \approx 0$) persists over a wider range of β.

For Newtonian fluids ($n = 1$) and $N = 2$, the optimal value $\beta^* = 0.71$ corresponds exactly to the prediction by Jing and Yi,[24] thereby validating our results. At the other extreme, for large radius ratios ($\beta \approx 1$), the rate of increase in conductance differs markedly with rheology. Specifically, shear-thickening fluids ($n > 1$) exhibit a much steeper increase in E_{vol} than shear-thinning fluids ($n < 1$).

Moreover, Figs. 5(a)–5(c) (varying γ) and Figs. 5(d)–5(f) (varying m) confirm that the optimal radius ratio $\beta^* = 0.71$ is independent of both the length ratio γ and the number of generations m, as well as the power-law index n. However, these parameters do influence the overall magnitude of the normalized electroosmotic conductance across *beta*, but the maximum value for $E_{\text{vol}} = 1$ at optimal condition β^* for all values of m, γ, and N. Considering networks with a radius ratio $\beta < 1$, the electroosmotic driving force, proportional to the surface area and zeta potential, accumulates across generations due to increased total surface exposure. Simultaneously, the viscous resistance also increases in successive generations as the effective hydraulic resistance of the network rises due to decreasing radii. The concurrent increase in both the electroosmotic driving force and the viscous resistance across generations leads to a balance. This balance keeps constant the maximum normalized electroosmotic conductance E_{vol} at an optimal branching configuration β^* as that of a single equivalent tube with $E_{\text{vol}} = 1$ as shown in all subfigures. It implies that branching networks can be designed to be just as efficient as a single straight tube in terms of electroosmotic transport despite having such complex geometry, thus establishing β^* as a universal design optimum under a volume constraint.

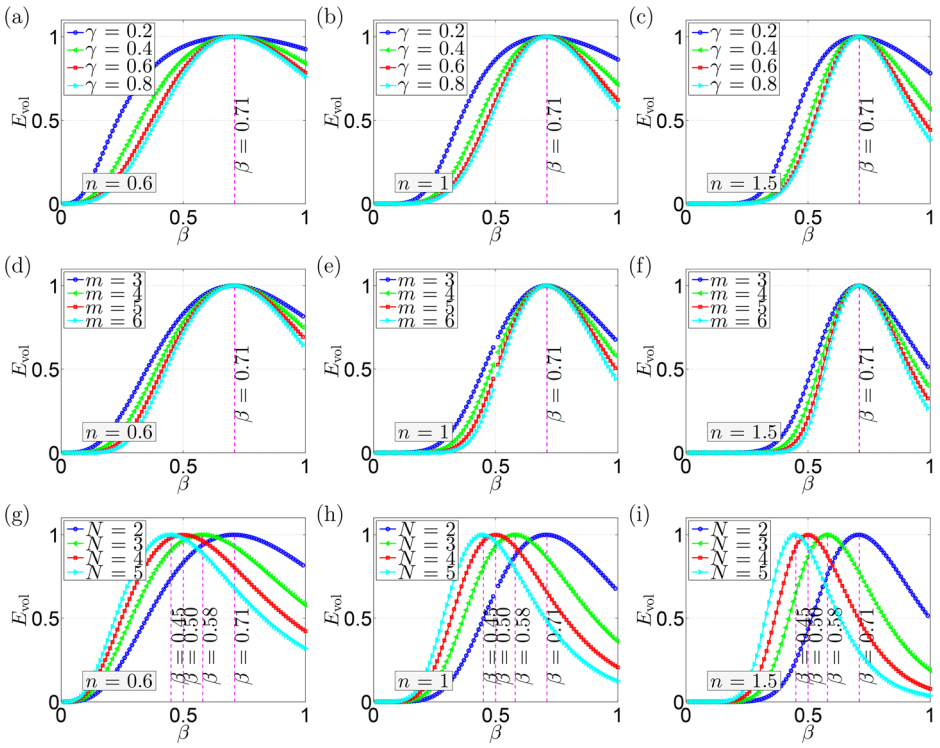

FIG. 5. We show the variation of the normalized electroosmotic conductance E_{vol} of the network with the dimensionless branching radius ratio β under volume constraint, for different parameter conditions. Subfigures (a)–(c) show the effect of varying the length ratio γ at fixed values of $m = 3$ and $N = 2$. Subfigures (d)–(f) illustrate the influence of the generation levels m, while keeping $N = 2$ and $\gamma = 0.5$. Subfigures (g)–(i) explore the impact of the number of branch splitting N at $m = 3$ and $\gamma = 0.5$. Each column corresponds to a different fluid rheology: shear-thinning fluids with $n = 0.6$ (a), (d), and (g), Newtonian fluids with $n = 1$ (b), (e), and (h), and shear-thickening fluids with $n = 1.5$ (c), (f), and (i).

Further analysis shows that, while the optimal β^* remains independent of γ and m for a fixed rheological index n, the optimal radius ratio β^* is sensitive to the bifurcation number N. As N decreases, the optimal β^* increases. Specifically, we observe $\beta^* = 0.45$, 0.50, 0.58, and0.71 for $N = 5$, 4, 3, and2, respectively, across all values of n. As the number of bifurcations N increases, β^* decreases with constant E_{max}.

2. Scaling laws and flow rate dependency

Figures 6(a)–6(c) show that the optimal branching radius ratio β^* corresponding to the maximum electroosmotic conductance E, systematically varies with the number of bifurcation branches N. The results, plotted on a log–log scale, reveal a power-law dependence of the form $\beta^* \propto N^{s_v}$, where s_v is the scaling exponent. Interestingly, this exponent remains constant at $s_v = -1/2$ across all values of the power-law index n, including shear-thinning, Newtonian, and shear-thickening fluids.

Using a similar analysis as performed by Garg,[34] Garg *et al.*,[35] we investigate the scaling of the optimal radius ratio β^* with the number of daughter branches N. We consider minimizing the total flow resistance [Eq. (34)] across a two-level (parent-daughter) branch at the kth level of a hierarchical electroosmotic network,

$$\mathcal{R}_{tot} = \sum_{i=k}^{k+1} \mathcal{R}_i = \frac{\eta_o \lambda_D^{1-n}}{\zeta \epsilon_o \epsilon_r (\pi n)^n} \left(\frac{L_k}{(N^n)^k R_k^{2n}} + \frac{L_{k+1}}{(N^n)^{k+1} R_{k+1}^{2n}} \right), \quad (43)$$

where η_0 is the consistency index, n is the power-law index, L_k and L_{k+1} are the lengths of the parent and daughter segments, and R_k, R_{k+1} being their corresponding radii. To minimize $\mathcal{R}_{tot}$ for a fixed fluid index n, we define

$$\mathcal{Z} = \frac{L_k}{(N^n)^k R_k^{2n}} + \frac{L_{k+1}}{(N^n)^{k+1} R_{k+1}^{2n}}, \quad (44)$$

to equivalently minimize subject to a volume constraint over the parent-daughter segment as

$$\mathcal{V} = \pi N^k R_k^2 L_k + \pi N^{k+1} R_{k+1}^2 L_{k+1}. \quad (45)$$

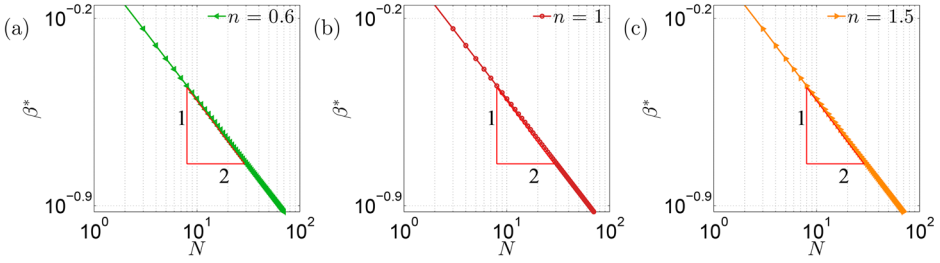

FIG. 6. Variation of the optimal radius ratio β^* as a function of the number of bifurcation branches N for different power-law index fluids on a log–log scale. Each subfigure [(a)–(c)] corresponds to a distinct power-law index: $n = 0.6$, 1, and 1.5, respectively. The results reveal a robust power-law scaling relationship $\beta^* \sim N^{s_v}$, where the scaling exponent $s_v = -1/2$ remains invariant across all fluid types.

Letting $x = R_k^2$ and $y = R_{k+1}^2$, we can substitute $y = (\mathcal{A} - \mathcal{B}x)$ using the volume constraint, where

$$\mathcal{A} = \frac{\mathcal{V}}{\pi N^{k+1} L_{k+1}}, \quad \mathcal{B} = \frac{L_k}{N L_{k+1}}.$$

Substituting into Eq. (44), we obtain

$$\mathcal{Z}(x) = \frac{L_k}{(N^n)^k x^n} + \frac{L_{k+1}}{(N^n)^{k+1}(A - Bx)^n}. \tag{46}$$

Setting the derivative $\frac{d\mathcal{Z}}{dx} = 0$, rearranging the terms and using the relation $R_{k+1}/R_k = \beta^\star$ yield

$$\beta^\star = \frac{R_{k+1}}{R_k} = N^{-1/2}. \tag{47}$$

This result indicates that the optimal radius ratio $\beta^\star$ is constant across all branching levels k, and thus applies to the entire network. Importantly, this optimal ratio is also independent of the length ratio $\gamma = L_{k+1}/L_k$, the branching depth m, and the power-law index n. Thus, the scaling $\beta^\star \propto N^{s_v}$ with $s_v = -1/2$ holds universally across all power-law fluids. The finding that $s_v = -1/2$ under a limiting scenario for the Newtonian fluids ($n = 1$) aligns well with previous results by Jing and Yi,[24] serving as a validation of our model. This universality in electroosmotic flows contrasts with pressure-driven flows, where the optimal scaling exponent appears as $s_v = -1/3$ under volume constraints, studied by Garg *et al.*,[35] showcasing different scaling laws across different flow-driving mechanisms.

Finally, we evaluate the scaling of the volumetric flow rate using this optimal ratio. From Eq. (47), we obtain

$$\left(\frac{Q_{k+1}}{Q_k}\right)^\star = \frac{1}{N} = \left(\frac{R_{k+1}}{R_k}\right)^2 \quad \Rightarrow \quad Q_k \propto R_k^2$$
under volume constraint for all n. (48)

Further, for a given electroosmotic flow and a fixed volumetric flow rate in an m-branched tree-like channel network, the parameters R_0, L_0, and m are constants. Under the total geometric volume constraint of the network, we have from Eq. (49)

$$\mathcal{V} = \pi R_0^2 L_0 \sum_{k=0}^{m} \left(N\beta^2\gamma\right)^k, \tag{49}$$

which implies that $N\beta^2\gamma$ must be a constant, denoted as χ. Now, at the optimal radius scaling for electroosmotic systems, which is $\beta^* \sim N^{-1/2}$, the volume constraint leads to

$$N\beta^2\gamma \sim N \cdot N^{-1} \cdot \gamma = \chi \Rightarrow \gamma \sim \chi,$$

where using a similar analysis as shown by Refs. 36 and 37 given in the Appendix, we can prove that $\chi = 1$ under optimal conditions.

Thus, the ratio of applied voltage between the daughter and parent branches is given by

$$\frac{\Delta V_{k+1}}{\Delta V_k} = \left(\frac{L_{k+1}}{R_{k+1}^{2n} Q_{k+1}^n}\right)\left(\frac{R_k^{2n} Q_k^n}{L_k}\right) = \frac{\gamma}{\beta^{2n} N^n}, \tag{50}$$

where we used the fact that $Q_{k+1}/Q_k = 1/N$. For Newtonian fluid, we get $\frac{\Delta V_{k+1}}{\Delta V_k} = \frac{\gamma}{\beta^2 N}$, same as shown by Ref. 24. At optimal conditions with $\beta^* = N^{-1/2}$ and $\gamma = \chi = 1$, we obtain

$$\left(\frac{\Delta V_{k+1}}{\Delta V_k}\right)_{\beta^*} = \chi = 1. \tag{51}$$

This result signifies an equipartition of voltage drops across each branching level under optimal electroosmotic flow conditions. Further, at optimal conditions, the mean velocity U_m scales as

$$\frac{Q_{k+1}}{Q_k} = \frac{U_{m,k+1} R_{k+1}^2}{U_{m,k} R_k^2}, \tag{52}$$

which implies

$$\frac{U_{m,k+1}}{U_{m,k}} = \frac{1}{N\beta^2} = 1. \tag{53}$$

This is another remarkable result, highlighting that under the optimal radius scaling $\beta^* = N^{-1/2}$ for electroosmotic flow, the mean velocity remains uniform across all levels of the branching network under volume constraint. To our knowledge, these scalings have not been reported before. Such uniformity in velocity distribution ensures efficient transport without velocity gradients that may cause dispersion or mixing inefficiencies.

Furthermore, the scaling relationship between the surface area and volume of the tube at the optimal flow condition, across successive levels in the parent-daughter network at the k^{th} level, is given by

$$\left(\frac{\mathcal{S}_{k+1}}{\mathcal{S}_k}\right)_{\beta^*} = \frac{R_{k+1} L_{k+1}}{R_k L_k} = N^{-1/2}, \tag{54}$$

while the corresponding volume ratio scales as

$$\left(\frac{\mathcal{V}_{k+1}}{\mathcal{V}_k}\right)_{\beta^*} = \frac{R_{k+1}^2 L_{k+1}}{R_k^2 L_k} = N^{-1}. \tag{55}$$

Combining these two relations yields the following elegant power-law relationship:

$$\frac{\mathcal{S}_{k+1}}{\mathcal{S}_k} = \left(\frac{\mathcal{V}_{k+1}}{\mathcal{V}_k}\right)^{1/2}. \tag{56}$$

This analysis highlights how the optimal radius ratio governs the scaling of geometrical quantities. Importantly, the optimal diameter ratio β^*, as well as the volume and surface area, are functions of the branching number N, and hence vary with network complexity. These results are crucial for the rational design of efficient tree-like flow networks under electroosmotic transport for power-law fluids.

B. surface-area constrained networks

In this section, we investigate the electroosmotic flow conductance E_{surf} in a tree-like circular tube network transporting power-law fluids, under the constraint of fixed total surface area of the network. Such a constraint is relevant in systems where surface-dominated phenomena (e.g., surface reactions, electroosmotic forces, and heat or mass transfer) are prominent in microfluidics transport systems. The analysis reveals how electroosmotic flow conductance is modulated by key parameters, such as fluid rheology, network geometry, and branching structure.

1. *Effect of* γ, m, *and* N

Figure 7 depicts the normalized electroosmotic conductance E_{surf} as a function of the branching radius ratio β, evaluated under fixed

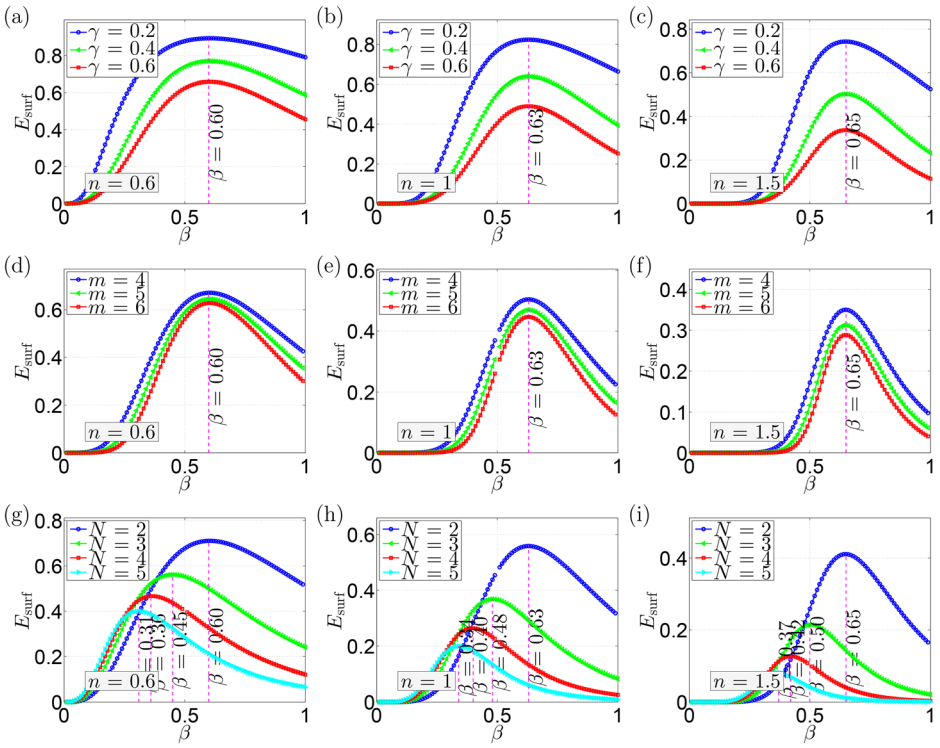

FIG. 7. We show the variation of normalized electroosmotic conductance E_{surf} of the network with the dimensionless branching radius ratio β under surface-area constraint, for different parameter conditions. Subfigures (a)–(c) show the effect of varying the length ratio γ at fixed values of $m = 3$ and $N = 2$. Subfigures (d)–(f) illustrate the influence of the generation levels m, while keeping $N = 2$ and $\gamma = 0.5$. Subfigures (g)–(i) explore the impact of the number of branch splitting N at $m = 3$ and $\gamma = 0.5$. Each column corresponds to different fluid rheology: shear-thinning fluids with $n = 0.6$ (a), (d), and (g), Newtonian fluids with $n = 1$ (b), (e), and (h), and shear-thickening fluids with $n = 1.5$ (c), (f), and (i).

surface area conditions. The figure presents results for varying axial length ratios γ (a)–(c), number of generations m (d)–(f), and the number of daughter branches N (g)–(i). The trends are shown for three types of fluids based on the flow behavior index n for shear-thinning [$n = 0.6$; (a), (d), (g)], Newtonian [$n = 1$; (b), (e), (h)], and shear-thickening fluids [$n = 1.5$; (c), (f), (i)].

The flow is driven by the electroosmotic force, while opposed by the viscous resistance. Figure 7 exhibits a non-monotonic dependence of the normalized electroosmotic conductance E_{surf} on the branching radius ratio β, indicating the presence of an optimal branching configuration β^* that maximizes conductance.

Similar to the flow characteristic under volume constraint, under surface area constraints, for small values of β (i.e., $\beta \to 0$), E_{surf} approaches zero across all values of the flow behavior index n, length ratio γ, generation number m, and bifurcation number N. In this regime, the viscous resistance overwhelmingly dominates, impeding electroosmotic transport. This low-conductance region extends over a broader β range as the fluid becomes more shear-thickening (increasing n), indicating a strong rheological influence.

As β increases, electroosmotic transport becomes more efficient. The trend is rheology-dependent as shear-thickening fluids ($n > 1$) exhibit a sharper rise in E_{surf} with β compared to Newtonian ($n = 1$) and shear-thinning ($n < 1$) fluids.

Figures 7(a)–7(c), which examine the influence of γ, and Figs. 7(d)–7(f), which vary m, confirm that the optimal radius ratio $\beta^* = 0.60$, 0.63, and 0.65 for $n = 0.6$, 1, and 1.5, respectively, show that with respect to the length ratio γ, and the number of generations m, β^* is invariant, however, depends on the rheological parameter n. While these parameters alter the overall magnitude of E_{surf}, the maximum normalized conductance decreases with all parameters flow behavior index n, length ratio γ, generation number m, and bifurcation number N unlike the maximum conductance $E_{vol} = 1$ remains unchanged under volume constraint. Further investigation reveals that while β^* is independent of γ and m for a given rheological index n, it is sensitive to the bifurcation number N. As N increases, the optimal radius ratio β^* decreases. We also find that β^* increases with n for all given parameters.

2. Scaling laws and flow rate dependency

Figures 8(a)–8(l) show that the optimal branching radius ratio β^* corresponding to the maximum electroosmotic conductance E systematically varies with the number of bifurcation branches N. The results, plotted on a log–log scale, reveal a power-law dependence of the form $\beta^* \propto N^{s_a}$, where s_a is the scaling exponent.

Using a similar analysis as performed by Garg,[34] Garg *et al.*,[35] we investigate the scaling of the optimal radius ratio $\beta^\star$ with the number of daughter branches N. We consider minimizing the total flow resistance [Eq. (34)] across a two-level (parent-daughter) branch at the kth level of a hierarchical electroosmotic network,

$$\mathcal{R}_{tot} = \sum_{i=k}^{k+1} \mathcal{R}_i = \frac{\eta_o \lambda_D^{1-n}}{\zeta \epsilon_o \epsilon_r (\pi n)^n} \left(\frac{L_k}{(N^n)^k R_k^{2n}} + \frac{L_{k+1}}{(N^n)^{k+1} R_{k+1}^{2n}} \right). \quad (57)$$

To minimize $\mathcal{R}_{tot}$ for a fixed fluid index n, we define

$$\mathcal{Z} = \frac{L_k}{(N^n)^k R_k^{2n}} + \frac{L_{k+1}}{(N^n)^{k+1} R_{k+1}^{2n}}, \quad (58)$$

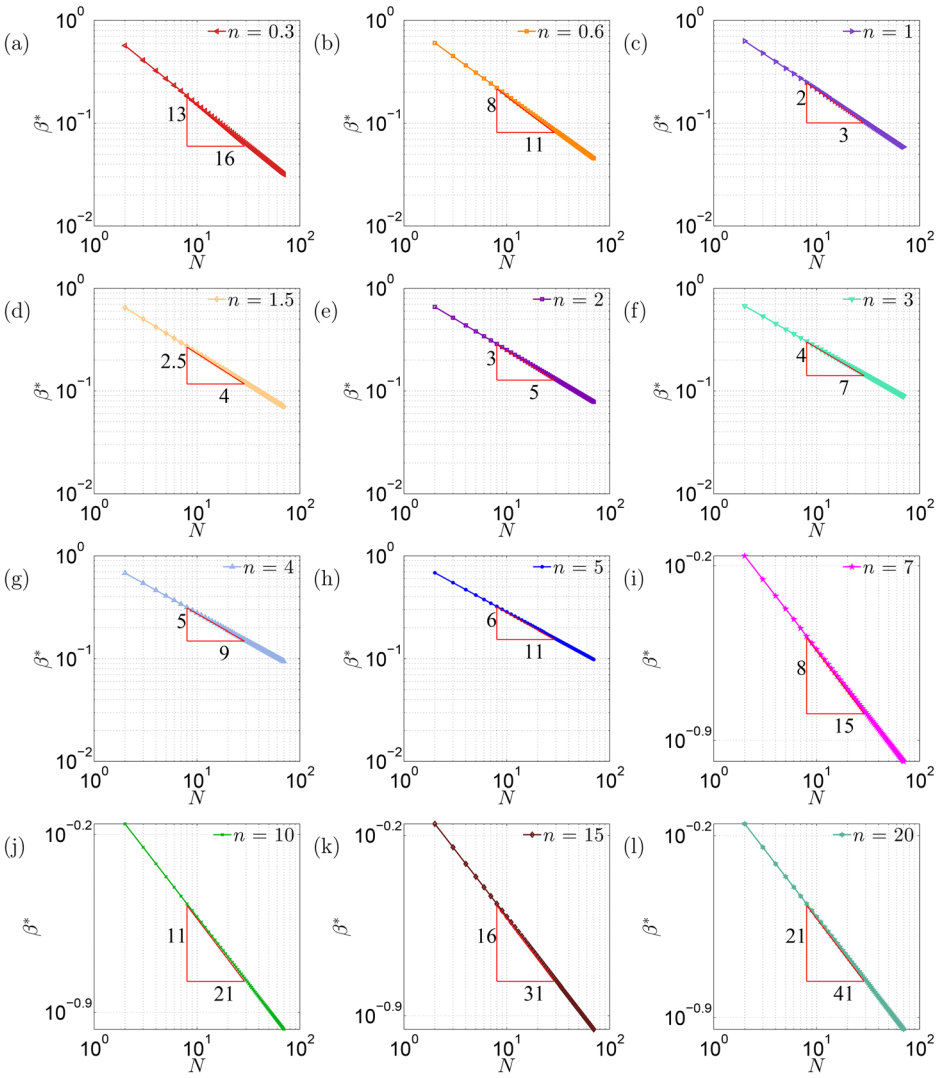

FIG. 8. Variation of the optimal radius ratio β^* as a function of branches splitting N for different power-law index n on a log–log scale.

to equivalently minimize subject to a fixed surface-area constraint over the parent-daughter segment as

$$\mathcal{S} = 2\pi N^k R_k L_k + 2\pi N^{k+1} R_{k+1} L_{k+1}. \tag{59}$$

Letting $x = R_k$ and $y = R_{k+1}$, we can substitute $y = (\mathcal{A} - \mathcal{B}x)$ using the surface-area constraint, where

$$\mathcal{A} = \frac{\mathcal{S}}{2\pi N^{k+1} L_{k+1}}, \quad \mathcal{B} = \frac{L_k}{N L_{k+1}}.$$

Substituting into Eq. (44), we obtain

$$\mathcal{Z}(x) = \frac{L_k}{(N^n)^k x^{2n}} + \frac{L_{k+1}}{(N^n)^{k+1}(A - Bx)^{2n}}. \tag{60}$$

Setting the derivative $\frac{d\mathcal{Z}}{dx} = 0$, rearranging the terms, and using the relation $R_{k+1}/R_k = \beta^*$ yield

$$\beta^* = \frac{R_{k+1}}{R_k} = N^{-(n+1)/(2n+1)}. \tag{61}$$

This result indicates that the optimal radius ratio β^* is constant across all branching levels k, and thus applies to the entire network. Importantly, this optimal ratio is independent of the length ratio $\gamma = L_{k+1}/L_k$, the branching depth m, however, varies with N and the power-law index n. So far, we have not come across such scaling law for electro osmotic flow for power law fluids under surface area constraint in any limiting scenario to validate. However, this law $s_a = -(n+1)/(2n+1)$ in electroosmotic flows, contrasts with pressure-driven flows, where the optimal scaling exponent appears as $s_a = -(n+1)/(3n+2)$ under surface-area constraints, studied by Garg *et al.*,[35] showcasing different scaling laws across different flow-driving mechanisms.

Finally, we evaluate the scaling of the volumetric flow rate using this optimal ratio. From Eq. (47), we obtain

$$\left(\frac{Q_{k+1}}{Q_k}\right)^* = \frac{1}{N} = \left(\frac{R_{k+1}}{R_k}\right)^{(2n+1)/(n+1)} \quad \Rightarrow \quad Q_k \propto R_k^{(2n+1)/(n+1)}$$
$$\text{under surface} - \text{area constraint.} \tag{62}$$

Further, for a given electroosmotic flow and a fixed volumetric flow rate in an m-branched tree-like channel network, the parameters R_0, L_0, and m are constants. Under the total geometric surface-area constraint of the network, we have from Eq. (63)

$$\mathcal{S} = 2\pi R_0 L_0 \sum_{k=0}^{m} (N\beta\gamma)^k, \tag{63}$$

which implies that $N\beta\gamma$ must be a constant, denoted as χ. Now, at the optimal radius scaling for electroosmotic systems, which is $\beta^* \sim N^{-(n+1)/(2n+1)}$, the surface-area constraint leads to

$$N\beta\gamma \sim N \cdot N^{-(n+1)/(2n+1)} \cdot \gamma = \chi \Rightarrow \gamma \sim \chi N^{(-n/(2n+1)},$$

where using a similar analysis as shown by Refs. 36 and 37, we can prove that $\chi = 1$ under optimal conditions.

Thus, the ratio of applied voltage between the daughter and parent branches is given by

$$\frac{\Delta V_{k+1}}{\Delta V_k} = \left(\frac{L_{k+1}}{R_{k+1}^{2n} Q_{k+1}^{n}}\right)\left(\frac{R_k^{2n} Q_k^n}{L_k}\right) = \frac{\gamma}{\beta^{2n} N^n}, \tag{64}$$

where we used the fact that $Q_{k+1}/Q_k = 1/N$. At optimal conditions with $\beta^* = N^{-(n+1)/(2n+1)}$ and $\gamma = \chi = 1$, we obtain

$$\left(\frac{\Delta V_{k+1}}{\Delta V_k}\right)_{\beta^*} = \chi = 1. \tag{65}$$

This result signifies an equipartition of voltage drops across each branching level under surface-area constraint at optimal electroosmotic flow conditions. Further, at optimal conditions, the mean velocity U_m scales as

$$\frac{Q_{k+1}}{Q_k} = \frac{U_{m,k+1} R_{k+1}^2}{U_{m,k} R_k^2}, \tag{66}$$

which implies

$$\frac{U_{m,k+1}}{U_{m,k}} = \frac{1}{N\beta^2} = N^{1/(2n+1)}. \tag{67}$$

This is another remarkable result, highlighting that at $\beta^* = N^{-(n+1)/(2n+1)}$ for electroosmotic flow, the mean velocity increases with bifurcation number N, however, it is in contrast to the pressure driven viscous flows, where it decreases with N.[35] To our knowledge, these scalings have not been reported before. Furthermore, the scaling relationship between the surface area and volume of the tube at the optimal flow condition, across successive levels in the parent-daughter network at the k^{th} level, is given by

$$\left(\frac{\mathcal{S}_{k+1}}{\mathcal{S}_k}\right)_{\beta^*} = \frac{R_{k+1} L_{k+1}}{R_k L_k} = N^{-1}, \tag{68}$$

while the corresponding volume ratio scales as

$$\left(\frac{\mathcal{V}_{k+1}}{\mathcal{V}_k}\right)_{\beta^*} = \frac{R_{k+1}^2 L_{k+1}}{R_k^2 L_k} = N^{-(3n+2)/(2n+1)}. \tag{69}$$

This analysis highlights how the optimal radius ratio governs the scaling of geometrical quantities. Importantly, the optimal diameter ratio β^*, as well as the mean velocity, geometrical volume, and surface area, are the functions of the branching number N and fluid index n, and hence vary with network complexity. These results are crucial for the rational design of efficient tree-like flow networks under electroosmotic transport for power-law fluids.

C. Critical evaluation of the study

The primary objective of this study was to derive and analyze scaling laws governing electroosmotic transport of power-law fluids without any limitation on the fluid index n in self-similar fractal branching microchannel networks, particularly under two practical constraints: total fluid volume and total surface area. The analytical approach provided closed-form relationships for key flow metrics such as mean velocity, conductance, and optimal branching ratio (β^*), evaluated across varying fluid rheologies characterized by the power-law index n.

The research findings comprehensively address the posed questions within the theoretical framework. Under the volume constraint, the model demonstrates that the optimal radius scaling $\beta^* = N^{-1/2}$ leads to uniform mean velocity across all generations and maximum normalized conductance ($E_{\text{vol}} = 1$), which holds independently of structural parameters, such as bifurcation number (N), length ratio (γ), and total generations (m). This result is robust and general, indicating a global performance optimum for a wide range of non-Newtonian fluids, including both shear-thinning and shear-thickening agents.

Under the surface-area constraint, however, the optimal radius ratio becomes a function of n, given by $\beta^* = N^{-(n+1)/(2n+1)}$. Here, the conductance E_{surf} can decrease significantly for higher values of n, reflecting increased viscous resistance and energy dissipation in shear-thickening fluids. While this outcome supports the theoretical model, it identifies a potential limitation in using such fluids in highly branched networks with restricted surface areas. This motivates future research on compensatory strategies for efficient flows, such as surface charge tuning, electrical field modulation, or hybrid electro-pressure schemes.

Minor deviations from ideal performance indicate that for certain n and N combinations, branching alone may not deliver optimal electrokinetic efficiency due to viscoplastic effects not captured in the shear-dependent viscosity model. Similarly, wall effects, electroviscous drag under high surface potential, or complex EDL structures may introduce deviations beyond the Debye–Hückel regime, suggesting directions for extension. Nonetheless, the presented framework provides a powerful baseline for predicting performance trends and guiding device optimization.

V. CONCLUSIONS

Electroosmotic flow (EOF) is a crucial mechanism for fluid transport in microfluidic systems, particularly when dealing with ionic solutions in micro- to nano-scale channels. This study presents a comprehensive analysis of electroosmotic flow (EOF) in fractal-like branching networks, focusing on power-law fluids and their behavior under volume and surface-area constraints. The research extends existing knowledge of EOF from single channels to complex, hierarchically branching networks, offering insights into scaling laws, flow resistance, and optimal branching configurations. The flow through the network is primarily driven by the applied electric field, while it is resisted by the viscous resistance due to fluid motion through the branched microchannels. By integrating fluid rheology with network geometry,

this work establishes universal design principles for efficient fluid transport in both natural and engineered systems.

The theoretical framework developed in this study models EOF in cylindrical microchannels filled with power-law fluids, accounting for electric double layers (EDL), zeta potential, and non-Newtonian fluid behavior. We assumed fully developed, axisymmetric, steady, and incompressible flow field. The EOF is modeled under the Debye–Hückel approximation, assuming low surface potential (i.e., thin electric double layer), no pressure gradient (purely electroosmotic). A combination of Poisson–Boltzmann for charge density and Navier–Stokes equations is used, adapted for EOF, and solved using boundary conditions tailored to branching geometries. The flow rate within the EDL is neglected in the analysis as it is a negligible comparison to the bulk flow rate of the channel. The resulting electroosmotic flow rates Q for power-law fluid enhance for shear-thinning fluids (lower n) compared to Newtonian or shear-thickening fluids. Further, the analysis demonstrates that under volume constraints, the optimal branching radius ratio β^* scales as $N^{-1/2}$, where N is the number of bifurcations. This scaling ensures uniform mean velocity across all levels of the network, highlighting the efficiency of electroosmotic transport. The results reveal that the normalized conductance E_{vol} reaches a constant maximum value of 1 under volume constraints, independent of any parameters such as length ratio γ, generations m, N, or n.

In contrast, under surface-area constraints, β^* scales as $N^{-(n+1)/(2n+1)}$, where n is the power-law index. For surface-area-constrained networks, the optimal β^* varies with fluid rheology n and N but remains invariant to γ and m. The maximum conductance E_{surf} decreases with increasing n, m, or N. The voltage drop across each generation remains the same under both volume and surface-area constraints at optimal conditions. Further, these scaling laws underscore the distinct characteristics of EOF compared to pressure-driven viscous flows. We further find that under optimal conditions, the volume and surface-area of each generation level are uniform under volume and surface-area constraints, respectively.

The integration of power-law fluid dynamics into fractal network models uncovers new optimization challenges. For example, in combined pressure-driven and electroosmotic flows, the optimal branch convergence ratio (β) transitions from $N^{-1/3}$ (pressure-dominated) to $N^{-1/2}$ (EOF-dominated) under volume constraint [$N^{-(n+1)/(3n+2)}$ (pressure-dominated) to $N^{-(n+1)/(2n+1)}$ (EOF-dominated) under surface-area constraint, respectively] as the voltage-to-pressure ratio increases. This transition is sensitive to network parameters such as length ratios (γ) and branching levels (m), with shear-thinning/thickening fluids exhibiting enhanced/reduced flow rates under AC/DC hybrid fields.

The implications of this research are significant for designing bio-inspired microfluidic devices, electrokinetic pumps, and lab-on-a-chip systems. The derived scaling laws provide a foundation for optimizing fluid transport in applications ranging from diagnostics to drug delivery.

Future work could refine the model by incorporating junction flow resistance and secondary flows at bifurcations. Extending the framework to non-Newtonian fluids with yield stress[38] or turbulent flow[39] regimes would broaden its applicability. Investigating asymmetric branching or charging configurations could also enhance its relevance for real-world engineering challenges.[21]

In conclusion, this study advances our understanding of EOF in complex geometries by integrating fluid rheology with fractal network design principles. The findings establish a robust theoretical foundation for optimizing electroosmotic transport in diverse systems while offering practical guidelines for engineering efficient microfluidic networks.

AUTHOR DECLARATIONS

Conflict of Interest

The authors have no conflicts to disclose.

Author Contributions

Ashish Garg: Conceptualization (equal); Data curation (equal); Formal analysis (equal); Funding acquisition (equal); Investigation (equal); Methodology (equal); Project administration (equal); Resources (equal); Software (equal); Supervision (equal); Validation (equal); Visualization (equal); Writing – original draft (equal); Writing – review & editing (equal).

DATA AVAILABILITY

All data generated and analyzed during this study are included within this manuscript.

APPENDIX: DERIVATION OF PRESSURE AND VOLUME PARTITIONING

The total geometrical volume constraint imposed on the fractal network is expressed as

$$V = \pi R_o^2 L_0 \sum_{k=0}^{m} \left(N\beta^2\gamma\right)^k, \tag{A1}$$

suggesting that $N\beta^2\gamma$ is assumed as χ. At $\beta^* = N^{-1/2}$, the $N\beta^2\gamma$ gives $\gamma = \chi$. Here, the parameter χ must be determined based on the total volume constraint of the network within a defined spatial domain. By applying Eqs. (57) and (45) at the optimal radius ratio β^*, the total hydraulic resistance of a single parent–daughter branching unit and its corresponding tube volume are given by

$$(\mathcal{R}_{\text{tot}})_{\beta^*} = \frac{\eta_o \lambda_D^{1-n}}{\zeta \epsilon_o \epsilon_r (\pi n)^n} \frac{1}{(N^n)^k R_k^{2n}} (L_k + L_{k+1}), \tag{A2}$$

and

$$(\mathcal{V})_{\beta^*} = \pi (N)^k R_k^2 (L_k + L_{k+1}), \tag{A3}$$

which yields

$$(\mathcal{R}_{\text{tot}} \mathcal{V}^n)_{\beta^*} = \frac{\eta_o \lambda_D^{1-n}}{\zeta \epsilon_o \epsilon_r (\pi n)^n} \frac{\pi^n}{(N^n)^k R_k^{2n}} (L_k + L_{k+1})^{n+1}. \tag{A4}$$

Furthermore, as proposed by Bejan *et al.*,[36] the planar spatial area $A_{s,k}$ in any direction in the k^{th} generation of the network, occupied by the branches of lengths L_k and L_{k+1} is related by

$$L_k L_{k+1} \propto A_{s,k} = \text{const.} \quad \Rightarrow \quad L_k L_{k+1} = \alpha_k A_{s,k}, \tag{A5}$$

where α_k is a proportionality constant at the k^{th} level. To minimize the total flow resistance $(\mathcal{R}_{\text{tot}})_{\beta^*}$ subject to the volume constraint $\mathcal{V}$, we optimize the lengths L_k and L_{k+1} under the spatial constraint

defined by the planar area $A_{s,k}$. From Eq. (A4), it is sufficient to minimize the functional Ψ, given by

$$\Psi = L_k + L_{k+1}, \tag{A6}$$

subject to the constraint in Eq. (A5). Applying the method of Lagrange multipliers, or direct minimization under this constraint, yields the optimal lengths as

$$L_k = (\alpha_k A_{s,k})^{1/2}, \tag{A7}$$

$$L_{k+1} = (\alpha_k A_{s,k})^{1/2}. \tag{A8}$$

From Eqs. (A7) and (A8), the length ratio at the optimal condition simplifies to

$$\gamma = \frac{L_{k+1}}{L_k} = 1, \tag{A9}$$

implying a constant value of $\chi = 1$. Substituting this into Eq. (51) confirms the equipartition of the applied voltage across each level. Moreover, $\chi = 1$ not only ensures voltage equipartition but also indicates equal volume distribution among branches across generations under volume constraint.

REFERENCES

[1]H. A. Stone, A. D. Stroock, and A. Ajdari, "Engineering flows in small devices: Microfluidics toward a lab-on-a-chip," Annu. Rev. Fluid Mech. **36**(1), 381–411 (2004).
[2]G. Karniadakis, A. Beskok, and N. Aluru, *Microflows and Nanoflows: Fundamentals and Simulation* (Springer, 2005).
[3]S. J. Lee and S. Lee, "Micro total analysis system (μ-tas) in biotechnology," Appl. Microbiol. Biotechnol. **64**(3), 289–299 (2004).
[4]J. Chen, M. Chu, K. Koulajian, X. Y. Wu, A. Giacca, and Y. Sun, "A monolithic polymeric microdevice for PH-responsive drug delivery," Biomed. Microdev. **11**(6), 1251–1257 (2009).
[5]J. Koo and C. Kleinstreuer, "Viscous dissipation effects in microtubes and microchannels," Int. J. Heat Mass Transfer **47**(14–16), 3159–3169 (2004).
[6]A. Alizadeh, W.-L. Hsu, M. Wang, and H. Daiguji, "Electroosmotic flow: From microfluidics to nanofluidics," Electrophoresis **42**(7–8), 834–868 (2021).
[7]G. E. Karniadakis, A. Beskok, and M. Gad-el Hak, "Micro flows: Fundamentals and simulation," Appl. Mech. Rev. **55**(4), B76–B76 (2002).
[8]B. Xiao, Y. Li, and G. Long, "A fractal model of power-law fluid through charged fibrous porous media by using the fractional-derivative theory," Fractals **30**(03), 2250072 (2022).
[9]S. Murtaza, P. Kumam, A. Kaewkhao, N. Khan, and Z. Ahmad, "Fractal fractional analysis of non linear electro osmotic flow with cadmium telluride nanoparticles," Sci. Rep. **12**(1), 20226 (2022).
[10]D. Jing and P. Qi, "The optimal branch width convergence ratio to maximize the transport efficiency of the combined electroosmotic and pressure-driven flow within a fractal tree-like convergent microchannel," Fractal Fract. **8**(5), 279 (2024).
[11]A. Abdelghany, K. Yamasaki, Y. Ichikawa, and M. Motosuke, "Efficient nanoparticle focusing utilizing cascade AC electroosmotic flow," Electrophoresis **43**(16–17), 1755–1764 (2022).
[12]S. Dehe, B. Rofman, M. Bercovici, and S. Hardt, "Electro-osmotic flow enhancement over superhydrophobic surfaces," Phys. Rev. Fluids **5**(5), 053701 (2020).
[13]A. Heeren, C. P. Luo, W. Henschel, M. Fleischer, and D. P. Kern, "Manipulation of micro- and nano-particles by electro-osmosis and dielectrophoresis," Microelectron. Eng. **84**(5–8), 1706–1709 (2007).
[14]A. Garg, N. Bergemann, B. Smith, M. Heil, and A. Juel, "Fluidisation of yield stress fluids under vibration," J. Non-Newtonian Fluid Mech. **294**, 104595 (2021).
[15]C. Zhao and C. Yang, "Analysis of power-law fluid flow in a microchannel with electrokinetic effects," Int. J. Emerg. Multidiscip. Fluid Sci. **1**, 37–52 (2009).
[16]R. P. Bharti, D. J. E. Harvie, and M. R. Davidson, "Electroviscous effects in steady fully developed flow of a power-law liquid through a cylindrical microchannel," Int. J. Heat Fluid Flow **30**(4), 804–811 (2009).
[17]N. Vasu and S. De, "Electroosmotic flow of power-law fluids at high zeta potentials," Colloids Surf. A **368**(1–3), 44–52 (2010).
[18]N. Vasu and S. De, "Electroviscous effects in purely pressure driven flow and stationary plane analysis in electroosmotic flow of power-law fluids in a slit microchannel," Int. J. Eng. Sci. **48**(11), 1641–1658 (2010).
[19]B. Srinivas, "Electroosmotic flow of a power law fluid in an elliptic microchannel," Colloids Surf. A **492**, 144–151 (2016).
[20]C. Zhao, W. Zhang, and C. Yang, "Dynamic electroosmotic flows of power-law fluids in rectangular microchannels," Micromachines **8**(2), 34 (2017).
[21]B. Mahapatra and A. Bandopadhyay, "Microconfined electroosmotic flow of a complex fluid with asymmetric charges: Interplay of fluid rheology and physicochemical heterogeneity," J. Non-Newtonian Fluid Mech. **289**, 104479 (2021).
[22]D. Jing and P. Qi, "Electroosmotic flow in fractal tree-like convergent microchannel network," Chem. Eng. Technol. **47**(6), 923–931 (2024).
[23]D. Jing and X. Zhan, "Cross-sectional dimension dependence of electroosmotic flow in fractal treelike rectangular microchannel network," Micromachines **11**(3), 266 (2020).
[24]D. Jing and S. Yi, "Electroosmotic flow in tree-like branching microchannel network," Fractals **27**(06), 1950095 (2019).
[25]D. Jing, L. He, and X. Wang, "Optimization analysis of fractal tree-like microchannel network for electroviscous flow to realize minimum hydraulic resistance," Int. J. Heat Mass Transfer **125**, 749–755 (2018).
[26]J. Kou, Y. Chen, X. Zhou, H. Lu, F. Wu, and J. Fan, "Optimal structure of tree-like branching networks for fluid flow," Physics A **393**, 527–534 (2014).
[27]W. Choi, S. Yun, and D.-S. Choi, "Electroosmotic flows of power-law fluids with asymmetric electrochemical boundary conditions in a rectangular microchannel," Micromachines **8**(5), 165 (2017).
[28]W. Choi, S. Yun, and D.-S. Choi, "Approximate solution for electroosmotic flow of power-law fluids in a planar microchannel with asymmetric electrochemical boundary conditions," Micromachines **9**(6), 265 (2018).
[29]C. D. Murray, "The physiological principle of minimum work: I. The vascular system and the cost of blood volume," Proc. Natl. Acad. Sci. U. S. A. **12**(3), 207–214 (1926).
[30]R. B. Bird, R. C. Armstrong, and O. Hassager, *Dynamics of Polymeric Liquids, Vol. 1: Fluid Mechanics* (John Wiley, 1987).
[31]A. Garg, "Pulsatile pressure enhanced rapid water transport through flexible graphene nano/angstrom-size channels: A continuum modeling approach using the micro-structure of nanoconfined water," New J. Phys. **25**(10), 103024 (2023).
[32]S. Chakraborty *et al.*, *Microfluidics and Microfabrication* (Springer-Verlag, Boston, 2010).
[33]C. Ll Rice and R. Whitehead, "Electrokinetic flow in a narrow cylindrical capillary," J. Phys. Chem. **69**(11), 4017–4024 (1965).
[34]A. Garg, "Scaling laws for optimal power-law fluid flow within converging–diverging dendritic networks of tubes and rectangular channels," Phys. Fluids **36**(7), 073116 (2024).
[35]A. Garg, H. Mishra, and S. K. Pattanayek, "Scaling laws for optimized power-law fluid flow in self-similar tree-like branching networks," J. Appl. Phys. **135**(20), 204702 (2024).
[36]A. Bejan, L. A. O. Rocha, and S. Lorente, "Thermodynamic optimization of geometry: T- and Y-shaped constructs of fluid streams," Int. J. Therm. Sci. **39**(9–11), 949–960 (2000).
[37]A. Garg and P. Prasad, "Yield–stress shear thinning and shear thickening fluid flows in deformable channels," Phys. Scr. **99**(3), 035240 (2024).
[38]A. Garg, "Scaling laws for optimal Herschel–Bulkley yield stress fluid flow in self-similar tree-like branching networks," Phys. Scr. **100**(3), 035920 (2025).
[39]A. Garg, H. Mishra, J. Sarkar, and S. K. Pattanayek, "Scaling laws for optimal turbulent flow in tree-like networks with smooth and rough tubes and power-law fluids," Eur. Phys. J. Plus **140**(2), 1–20 (2025).